ACS APPLIED MATERIALS & INTERFACES

Research Article

www.acsami.org

Nanosheet-Assembled NiO Microstructures for High-Performance Supercapacitors

Kamatchi Kamaraj Purushothaman,*[,†] Inbamani Manohara Babu,[†] Balasubramanian Sethuraman,[†] and Gopalan Muralidharan[‡]

[†]Department of Physics, TRP Engineering College (SRM Group), Irungalur, Tamilnadu, India

[‡]Department of Physics, Gandhigram Rural University, Gandhigram-624302, Tamilnadu, India

Supporting Information

ABSTRACT: Nanosheet-assembled NiO microstructures have been synthesized via a hydrothermal method. The presence of anionic surfactant in the fabrication process initiates the formation of lamellar micelles and a self-assembling process. This leads to the formation of NiO nanosheets and organizes it into microstructures. The effect of preparation temperature on the morphological, structural, and electrochemical properties and stability upon continuous charge/discharge cycles has been examined for supercapacitor applications. Electrochemical analysis demonstrated that NiO nanosheets prepared at 160 °C are capable of delivering a specific capacitance of 989 F g^{-1} at a scan rate of 3 mV s^{-1} for the potential window of 0−0.6 V. The nanosheets exhibit excellent capacity retention, 97% retention after 1000 continuous charge/discharge cycles, and an energy density of 49.45 W h kg^{-1}.

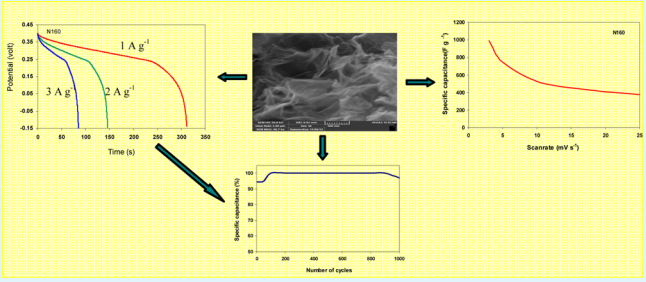

KEYWORDS: *supercapacitor, nanosheets, nickel oxide, hydrothermal, self-assembling*

1. INTRODUCTION

Over the past decade, supercapacitors have attracted much attention, because of their long cycle life, short charging time, high power density, etc.[1] They find use in a variety of applications, such as portable electronic devices, micro electromechanical systems, and hybrid electric vehicles. They provide power during peak power demand in conjunction with batteries.[2] Depending on the energy storage mechanism, electrochemical capacitors can be divided into electric double layer capacitors (EDLCs) and pseudo-capacitors. Carbon materials with high surface area such as carbon nanotubes, graphene, and porous carbon exhibit EDLC behavior, where charges are stored at the interface between the electrode and the electrolyte. The large-scale application of EDLCs is limited by their low specific capacitance (100−200 F g^{-1}). The pseudo-capacitors employ transition-metal oxides (RuO_2, Co_3O_4, MnO_2, NiO, ...) and/or conducting polymers (PANI, PPy, PEDOT, ...) as the electrode materials. These undergo fast reversible Faradic redox reaction and result in a specific capacitance 10−100 times higher than that of EDLCs.[3,4] Among the various transition-metal oxides, nickel oxide has attracted the greatest amount of attention, because of its high theoretical capacity (2573 F g^{-1} within 0.5 V), low cost, low toxicity, low environmental impact, and sufficiently large pseudo-capacitive behavior (comparable to that of RuO_2).[5,6]

Nanostructured materials with intrinsically large surface area have been reported to show improved electrochemical properties at high charge/discharge rates. Because of the complicated fabrication process, the preparation of novel nickel oxide architectures, which exhibit remarkable electrochemical performance, remains a significant challenge. Nanostructured NiO materials have been prepared via various methods, such as sol−gel, hydrothermal, hard template, electrodeposition, and microwave-assisted synthesis.[7−11] The hydrothermal method is facile to the synthesis of NiO materials with controlled morphologies and porous structures.

The electrochemical behavior of NiO depends, to a larger extent, on the surface morphology, porosity, and surface area. Xing et al. reported a specific capacitance of 124 F g^{-1} at a current density of 100 mA g^{-1} for spherical mesoporous NiO.[12] Polyhedron-shaped NiO[13] were reported to exhibit a specific capacitance of 165 F g^{-1} at a scan rate of 5 mV s^{-1}. NiO in the form of nanowires[14] and hexagon plates[15] respectively yielded a specific capacitance of 120 F g^{-1} at a current density of 1 mA cm^{-2} and a specific capacitance of 72 F g^{-1} at a current density of 1.5 mA cm^{-2}.

The primary focus of current researchers is to develop nanostructured materials with different structural arrangements. Some of these arrangements lead to inadequate charge transport that limits the rate capability of electrodes, although they have high specific area. Among the nanostructured materials, the nanosheet-assembled microstructures are better

Received: July 21, 2013
Accepted: October 14, 2013
Published: October 14, 2013

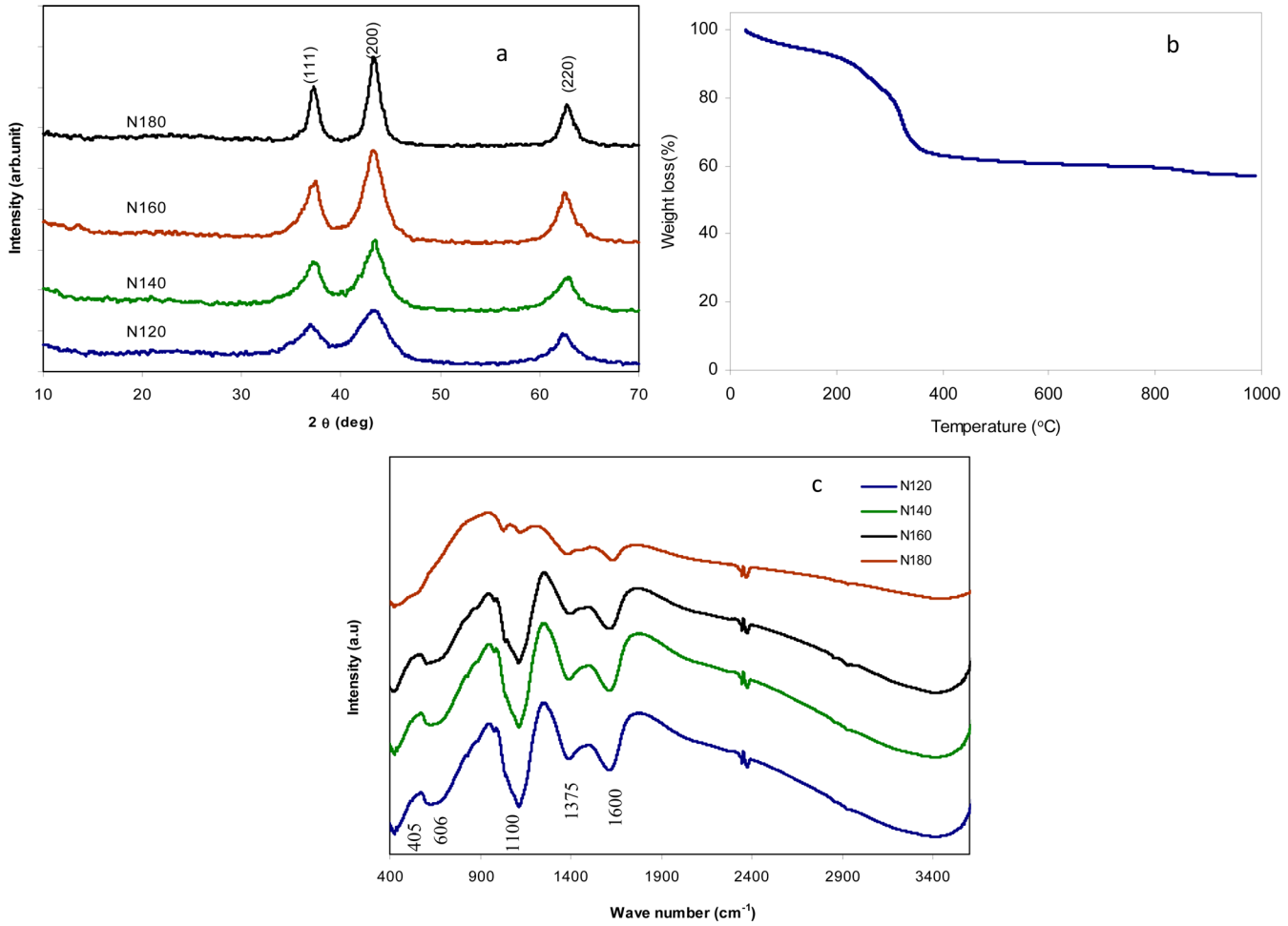

Figure 1. (a) X-ray diffraction (XRD) patterns of NiO prepared at different temperatures, (b) thermogravimetric analysis (TGA) of the as-prepared sample (160 °C), and (c) Fourier transform infrared (FTIR) spectra of N120, N140, N160, and N180.

candidates, because they provide more paths for the diffusion of electrolyte ions, which enables enhanced electochemical performance of the electrode material. In this paper, we report the formation of NiO porous microstructures by self-assembling nanosheets prepared via the hydrothermal method, using SDS as a surfactant. The effect of preparation temperature on the structural, morphological, and electrochemical properties of self-assembled NiO microstructures has been reported and discussed.

2.0. EXPERIMENTAL DETAILS

2.1. Material Synthesis. Analytical-grade nickel nitrate hexahydrate ($NiNO_3{\cdot}6H_2O$), urea, and sodium dodecyl sulfate (SDS) were used as purchased without further processing. In a typical synthesis, 0.1081 g of SDS was dissolved in 50 mL of double distilled water; 0.4362 g of $NiNO_3{\cdot}6H_2O$ was dissolved in 15 mL of water. This solution was added slowly to the SDS solution under constant stirring at room temperature; 0.1801 g of urea dissolved in 10 mL of water was added to the solution containing SDS and $NiNO_3{\cdot}6H_2O$. The resultant solution was continuously stirred for 2 h. The solution thus obtained was transferred to a 100-mL Teflon-lined stainless steel autoclave and was kept at 120, 140, 160, and 180 °C, respectively, for 24 h. A solid green product was obtained by centrifugation. This product was repeatedly washed with ethanol and double distilled water. NiO has been obtained by annealing the green powder at 300 °C for 2 h in an air atmosphere. The products were ultimately named N120, N140, N160, and N180, respectively. For example, N120 would correspond to the material prepared at 120 °C.

2.2. Material Characterization. X-ray diffraction (XRD) analysis was performed from 10° to 80°, using a PANalytical XPERT- PRO X-ray diffractometer with Cu Kα radiation to determine the phase and purity of the samples. The Debye−Scherrer formula has been used to estimate the grain size of the NiO samples. Fourier transform infrared (FTIR) spectra have been recorded using Perkin−Elmer SPECTRUM BX II equipment, while thermogravimetric analysis (TGA) was made using Universal V4.7A system (TA Instruments, model SDT Q600), at a heating rate of 20 °C min^{-1}. Surface morphology of the NiO samples was recorded using scanning electron microscopy (SEM) (Model TESCAN VEGA-3 LMU).

2.3. Electrode Preparation and Electrochemical Measurement. The electrochemical performance of NiO nanostructures was studied using three electrode cell configurations with NiO as the working electrode, platinum wire as the counter electrode, Ag/AgCl as the reference electrode, and 2 M KOH as the electrolyte. The working electrode was prepared by mixing 85 wt % NiO, 10 wt % activated carbon, and 5 wt % polytetrafluoroethlene (PTFE), along with a few drops of ethanol. This slurry was coated onto nickel foam with an area of 1 cm^2. Finally, the electrode was dried at 80 °C for 8 h. Cyclic voltammetry (CV), galvanostatic charge/discharge, and electrochemical impedance spectroscopy (EIS) measurements were carried out using a CHI Model 660 D electrochemical workstation. The CV analysis was performed at different scan rates in the potential window of 0−0.6 V. The galvanostatic charge/discharge measurements were carried out in the potential range from −0.15 V to 0.4 V for different current densities. EIS measurements were made between 0.01 Hz and 100 kHz, with an amplitude of 5 mV.

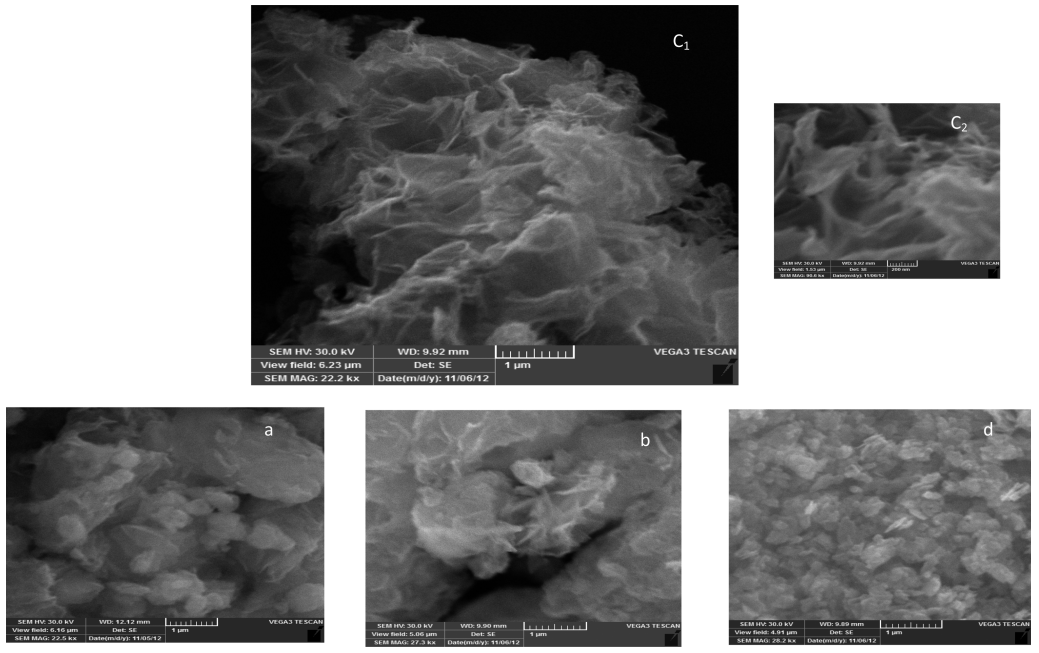

Figure 2. SEM images of the samples: (a) N120, (b) N140, (c1,c2) N160, and (d) N180.

Scheme 1. Formation Mechanism of a NiO Nanosheet-Assembled Microstructure

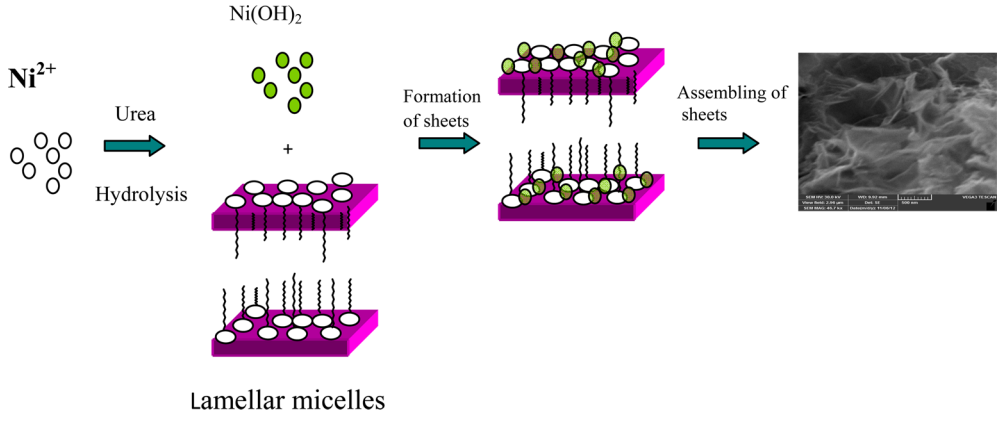

3.0. RESULTS AND DISCUSSION

3.1. Structural, Thermal, and Morphological Studies. The phase structure and purity of the prepared powders were examined by powder XRD. NiO samples revealed well-resolved diffraction peaks at 37.2°, 43.2°, and 62.7° (see Figure 1), which can be indexed as the peak corresponding to the (111), (200), and (220) planes of cubic NiO structure (JCPDS File Card No. 78-0643). No additional peaks were observed, indicating the high degree of phase purity of the NiO prepared in this work. The diffraction peaks in all four cases (N120–N180) show broad bands, indicating the mesoscopic nature of the crystallites. The diffraction peaks become sharper when the preparation temperature increases from 120 °C to 180 °C. The particle size, as obtained from XRD, was in the range of 8–16 nm.

Phase change and decomposition of the as-prepared sample (160 °C) were studied using the TGA method. Three steps of weight loss could be observed (Figure 1b): (i) room temperature (RT) to 200 °C, (ii) 200–355 °C, and (iii) 400–1000 °C. The sharp weight loss at ∼350 °C is indicative of the formation of NiO. Figure 1c shows the FTIR spectra of the N120, N140, N160, and N180 samples. The vibrational bands are observed at ∼405, 606, 1100, 1375, and 1600 cm^{-1}. The band centered at 1600 cm^{-1} is attributed to the bending mode of vibration of residual water (O–H).[16] The band at 1375 cm^{-1} corresponds to interlayer NO_3^- molecule.[17] The bands observed at ∼1100 cm^{-1} and 606 cm^{-1} are due to the sulfate headgroup (SO_4^{2-}) in the SDS. The band at 405 cm^{-1} corresponds to the stretching vibration of NiO.[18] Now we are able to conclude that the weight loss at RT–200 °C is due to the removal of water and alkyl chain of surfactant SDS. The weight loss of ∼27%, which has been observed in the second step (200–355 °C), corresponds to the conversion of $Ni(OH)_2$ to NiO. The minor weight loss that occurs between 400 °C and 600 °C is due to the removal of the sulfate headgroup in the SDS.[19] The FTIR spectra of samples annealed at 300 °C shows SO_4^{2-} vibrations, and the formation of NiO is confirmed by XRD.

SEM images are shown in Figure 2. SEM images showed the formation of hierarchical microspheres for the N120 and N140 samples (see Figure S1 in the Supporting Information). Two-dimensional (2D) nanosheet arrays interwoven together to form a three-dimensional (3D) structure has been observed for

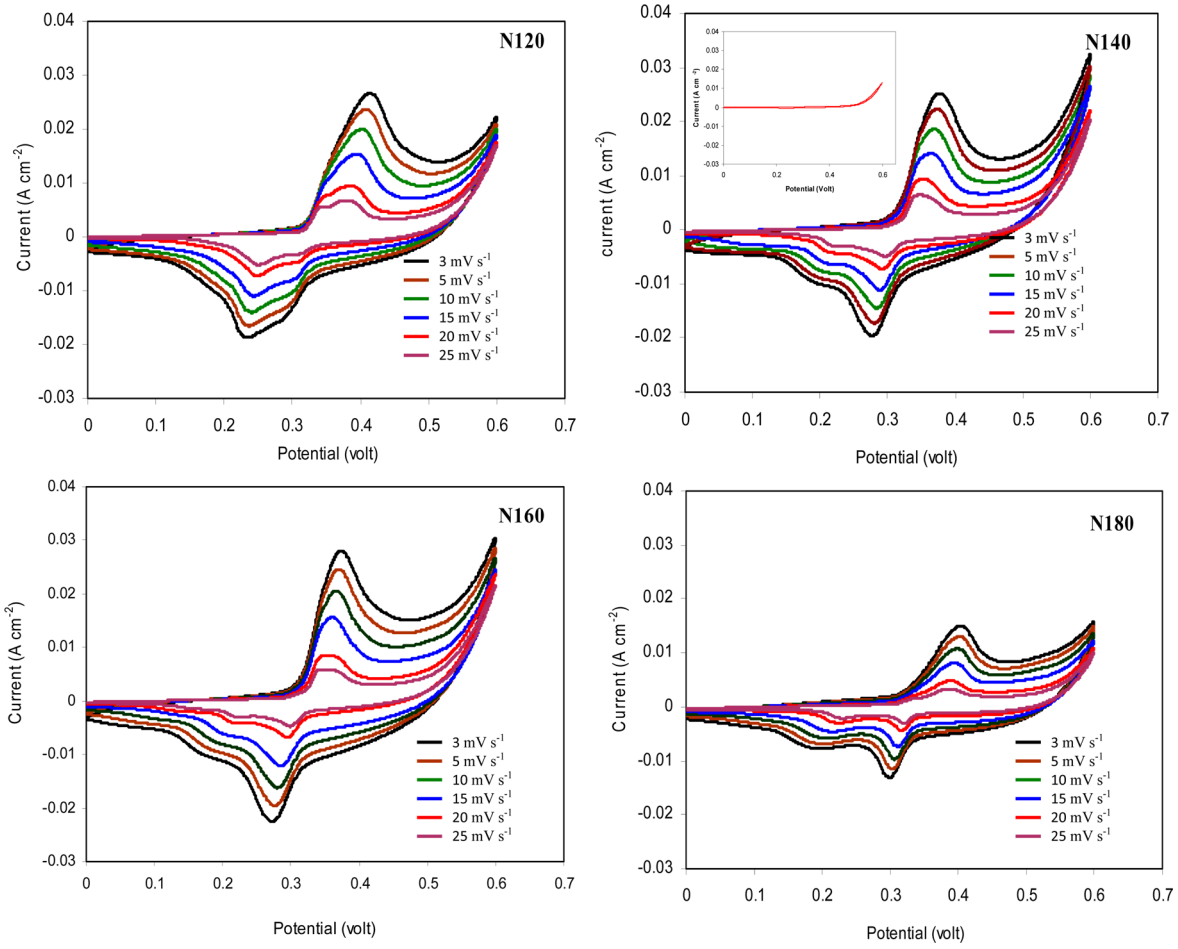

Figure 3. Cyclic voltammetry (CV) curves of the N120, N140, N160, and N180 samples at different scan rates. Inset in the panel for the N140 sample shows the CV curve of nickel foam at 3 mV s^{-1}.

the N160 sample. The N180 sample exhibits a platelike morphology, because of the agglomeration of nanorods (see Figure S1 in the Supporting Information). Scheme 1 shows the possible mechanism of formation of NiO nanosheets. A sheetlike structure has been formed because of the presence of an anion surfactant, which results in the formation of lamellar micelles, and these nanosheets assemble together to form microscaled architectures. At the initial stage of the hydrothermal process, $Ni(OH)_2$ is formed by the hydrolysis of urea. Different reaction temperatures lead to different rates of nucleaetion and growth rate of $Ni(OH)_2$. At 120 and 140 °C, the assembly of nanosheets is slow and, hence, they probably assemble into microspheres under the assistance of a surfactant. A decrease in the surface tension with increasing preparation temperature results in weak electrostatic interaction. The reduced surface tension lowers the aggregation, enabling the formation of microspheres with well-resolved nanosheets at 160 °C. The initial nucleation and growth rate will be faster at 180 °C. The faster nucleation hinders the assembly of anion surfactant and cation, resulting in the formation of nanorod-assembled thicker plates. Kuang et al.[20] reported the formation of nanosheets at 120 °C and thick nanoplates at 180 °C. Liu et al.[21] reported step-by-step variations of morphology, from a joint sheetlike structure to smooth rods, while varying the temperature from 120 °C to 180 °C in steps of 20 °C.

3.2. Electrochemical Studies. CV analysis has been performed for the electrodes prepared in this work in the potential range of 0−0.6 V, using 2 M KOH as the electrolyte. Figure 3 shows the CV curves of the N120, N140, N160, and N180 samples at different scan rates; the inset shows the CV curve of nickel foam at 3 mV s^{-1}. The shape of the CV curves is different from the ideal rectangular shape (because of electric double layer capacitance), indicating that the electrodes in the current work exhibit pseudo-capacitance behavior. The CV curves reveal a pair of distinct redox peaks, which suggest the pseudo-capacitance nature of NiO. The charge storage of NiO arises from the following redox equation:[22]

$$NiO + zOH^- \Leftrightarrow zNiOOH + (1 - z)NiO + ze^- \quad (1)$$

The specific capacitance (C_s) values are calculated using the equation[23]

$$C_s = \frac{I}{mv} \quad (2)$$

where I is the average current (A) during the anodic and cathodic sweep, m the mass of the electrode material (g), and v the voltage sweep rate (V). The N120 sample exhibited a specific capacitance of 871 F g^{-1}, while the same for N140 was 925 F g^{-1}. The maximum specific capacitance of 989 F g^{-1} was obtained for the N160 sample while the specific capacitance showed a reduced value of 496 F g^{-1} for the N180 sample. These values were obtained at a scan rate of 3 mV s^{-1}. The formation of a nanosheet-like structure seem to have facilitated the ion exchange process by reducing the diffusion lengths for

the electrolyte, yielding a superior redox process in the case of the N160 sample, which exhibited the best specific capacitance. The specific capacitance, as observed with the N180 sample (the samples prepared at 180 °C), was lower compared to the N160 sample; at elevated temperatures, crystallites of larger size are formed, and they limit the paths available for ion transport. Figure 4 shows the specific capacitance as a function of scan rate. Specific capacitance decreases with increasing scan rate. At higher scan rates, the accessible surface of the active material by the ions are limited, while at the lower scan rates, it will utilize the inner surface as well as the outer surface and leads to an increase in the capacitance.[24]

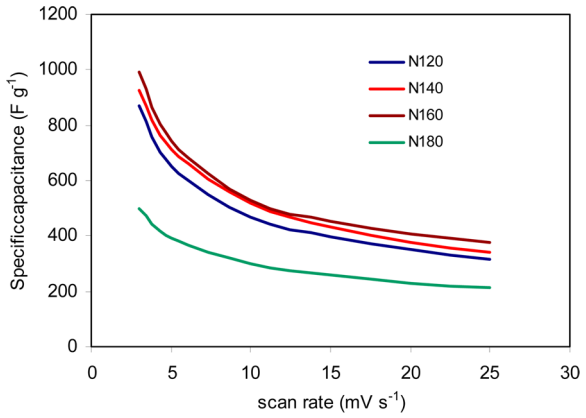

Figure 4. Specific capacitance as a function of scan rate.

Galvanostatic charge/discharge (GCD) studies have been performed to estimate the specific capacitance and to evaluate the cyclic stability of the electrode materials prepared in the present work. The GCD measurements were carried out in 2 M KOH solution between −0.15 V and 0.4 V at different current densities, from 1 A g^{-1} to 3 A g^{-1}. Figure 5 shows the discharge curves of the N120, N140, N160, and N180 samples. The specific capacitance (C_s) has been calculated using the following relation:[25]

$$C_s = \frac{I\Delta t}{m\Delta v} \quad (3)$$

where I is the discharging current (mA), Δt the discharging time (s), m the mass of the electrode material (g), and Δv the discharging potential range (V). The C_s values of the N120, N140, N160, and N180 samples are 507, 525, 567, and 420 F g^{-1}, respectively, at 1 A g^{-1}. The N160 sample also exhibits the highest specific capacitance in this case. A C_s value of 282 F g^{-1} at 0.5 A g^{-1} has been reported by Justin et al.[8] for the porous NiO nanoflake-like morphology prepared via the hydrothermal method. Zheng et al.[26] reported a C_s value of 132 F g^{-1} at 0.5 A g^{-1} for NiO nanoflakes. Compared to these reports, we observed that the N160 sample offers a higher specific capacitance (near 100% improvement) at current densities twice as high. Note that better C_s values are obtained at lower current densities. At high current densities, the IR drop is high

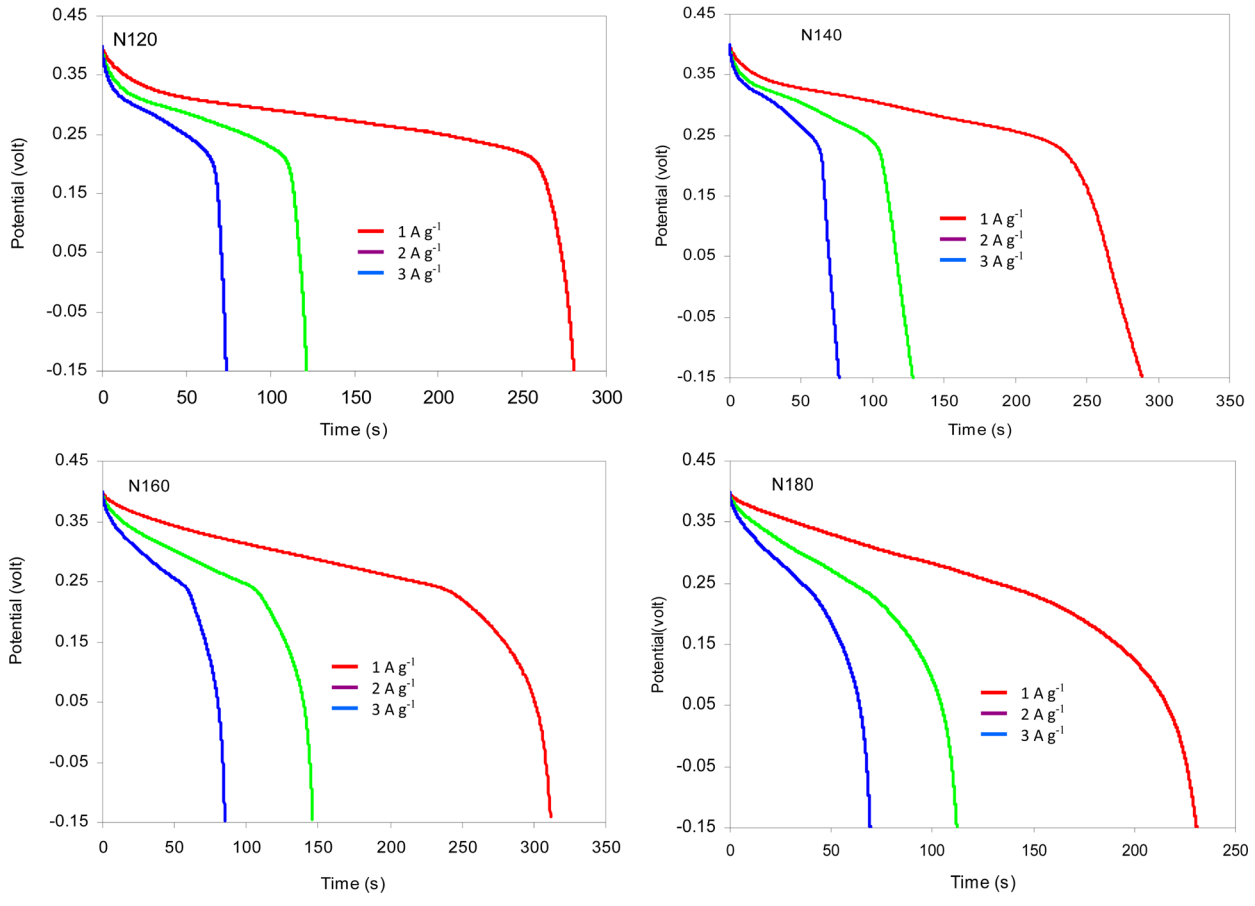

Figure 5. Discharge curves for the N120, N140, N160, and N180 samples at different current densities.

dx.doi.org/10.1021/am402869p | ACS Appl. Mater. Interfaces 2013, 5, 10767−10773

and it decreases the C_s value, while at low current densities, the IR drop is small.[27]

The utilization factor of NiO electrodes has been calculated using the following equation:[28]

$$z = \frac{C\Delta VM}{F} \quad (4)$$

where C is the specific capacitance (F g^{-1}), ΔV the potential window, M the molecular weight of NiO (74.692 g), and F the Faradic constant. A value of $z = 1$ indicates that the entire electroactive material is involved in the redox reaction. The z values for the N120, N140, N160, and N180 samples are 0.215, 0.224, 0.241, and 0.179, respectively. In the N160 sample electrode, 24.1% of the electroactive material is involved in the redox reaction and results in the maximum specific capacitance.

Achieving high energy density in the pseudo-capacitive material is a challenging task for researchers. Increasing the potential or capacitance leads to higher energy densities. The energy density values are calculated using the equation

$$E = \frac{1}{2}CV^2 \quad (5)$$

where C is the specific capacitance and V is the potential window. The N120, N140, N160, and N180 samples exhibit energy densities of 43.55, 47.6, 49.45, and 24.8 W h kg^{-1}, respectively, at 3 mV s^{-1}. The N160 sample exhibits the maximum energy density and that is in the range of nickel metal hydride batteries.[29]

The stability of the electrode has been tested by cyclic charge/discharge analysis to explore the service life of the capacitor for their practical applications. Figure 6 shows the

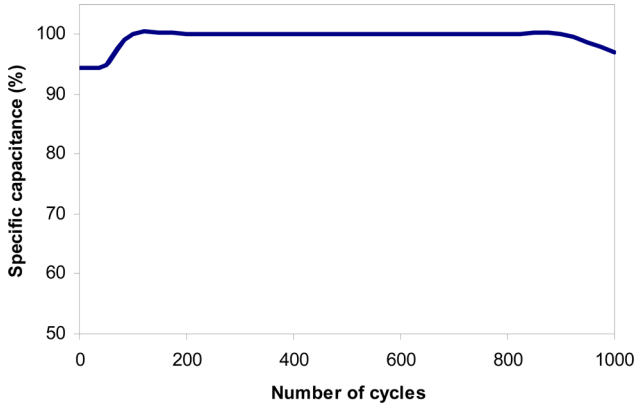

Figure 6. Capacitance retention with continuous charge/discharge cycles of the N160 sample at 3 A g^{-1}.

specific capacitance as a function of number of cycles for the N160 sample. No degradation could be observed up to 900 cycles. Furthermore, we see that 97% of maximum capacity is retained, even after 1000 cycles. Vijayakumar et al.[11] reported the capacitive retention to be 92% after 500 cycles for NiO nanoflakes. In their work on C@NiO composites, Fan et al.[30] reported 90.7% retention after 1000 cycles. Xu et al.[31] observed a 3.2% decrease in the specific capacitance after 500 cycles. From these reports, we conclude that the electrodes prepared in the work are better, because they exhibit better stability and higher specific capacitance.

EIS measurements were made to identify the resistive and capacitive elements, which decide the electrochemical performance of the electrode. Figure 6 shows the Nyquist plot for the N120, N140, N160, and N180 samples in the frequency range from 0.01 Hz to 100 kHz at an amplitude of 5 mV versus the potential of 0.3 V. The EIS data were fitted to an equivalent circuit consisting of a solution resistance R_s, a charge-transfer resistance R_{ct}, a double layer capacitance C_{dl}, pseudo-capacitance C_p, and the Warburg impedance W. The circuit is shown in the inset of Figure 7. The Nyquist plot can be

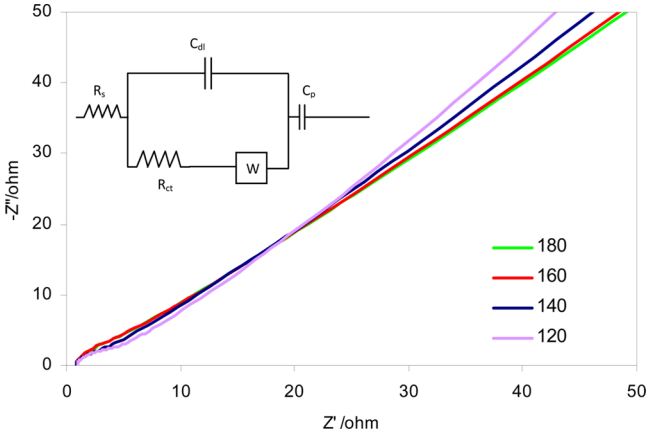

Figure 7. Impedance plot of the N120, N140, N160, and N180 samples at 0.4 V; inset shows the equivalent fitting circuit.

resolved into a high-frequency component (partial semicircle) and a low-frequency component (straight sloping line along an imaginary axis). The R_s and R_{ct} values can be calculated from the intercepts of a high-frequency semicircle on the real axis at R_s and $R_s + R_{ct}$, respectively. R_s is the combination of ohmic resistance of electrolyte and internal resistance of the electrode material. The solution resistance of the N120, N140, N160, and N180 samples are 0.63, 0.67, 0.79, and 0.92 Ω, respectively, while the R_{ct} values are 6.71, 6.03, 5.57, and 5.72 Ω in the same order. The N160 sample exhibits the lower R_{ct} value, making it a better candidate for higher uptake and delivery applications. The charge-transfer resistance is related to the electrolyte accessible area of the electrode and is called the Faraday resistance; this is a limiting factor for the specific power of a supercapacitor.[32,33]

4. CONCLUSION

Microspheres with self-assembled nanosheets were synthesized by a facile and cost-effective hydrothermal method using sodium dodecyl sulfate as the surfactant. The nanosheet arrays with open paths (represented by the N160 sample) lead to fast ion transportation, and excellent electrolyte infiltration results in a specific capacitance of 989 F g^{-1} and an energy density of 49.45 W h kg^{-1} with a charge-transfer resistance of 5.57 Ω. Excellent capacity retention (97%), as well as low charge-transfer resistance, make the N160 sample a promising electrode material for supercapacitor applications.

■ ASSOCIATED CONTENT

Supporting Information

SEM images for N120, N140, N160, and N180 (Figure S1). This material is available free of charge via the Internet at http://pubs.acs.org.

AUTHOR INFORMATION

Corresponding Author

*Tel.: +91 431 2908050. E-mail: purushoth_gri@yahoo.co.in.

Notes

The authors declare no competing financial interest.

ACKNOWLEDGMENTS

One of the authors (K.K.P.) thanks Department of Science and Technology-SERC, New Delhi, India, for providing the financial support under Young Scientist Scheme and Nanotechnology Research Centre, SRM University, Kattankulathur, India, for providing XRD facility.

REFERENCES

(1) Simon, P.; Gogotsi, Y. *Nat. Mater.* **2008**, *20*, 845−854.
(2) Deng, W.; Ji, X.; Chen, Q.; Banks, C. E. *RSC Adv.* **2011**, *1*, 1171−1178.
(3) Wang, G.; Zhang, L.; Zhang, J. *Chem. Soc. Rev.* **2012**, *41*, 797−828.
(4) Conway, B. E. *J. Electrochem. Soc.* **1991**, *138*, 1539−1548.
(5) Yuan, C.; Zhang, X.; Su, L.; Gao, B.; Shen, L. *J. Mater. Chem.* **2009**, *19*, 5772−5777.
(6) Bi, R. R.; Wu, X. L.; Gao, F. F.; Jiang, L. Y.; Guo, Y. G.; Wan, L. J. *J. Phys. Chem.* **2009**, *19*, 5772−5777.
(7) Lu, K. C.; Anderson, M. A. *J. Electrochem. Soc.* **1996**, *143*, 124−130.
(8) Justin, P.; Meher, S. K.; Rao, G. R. *J. Phys. Chem. C* **2010**, *114*, 5203−5210.
(9) Ding, S.; Zhu, T.; Chen, J. S.; Wang, Z.; Yuan, C.; Lou, X. W. *J. Mater. Chem.* **2011**, *21*, 6602−6606.
(10) Wu, M. S.; Wang, M. J.; Jow, J. J. *J. Power Sources* **2010**, *195*, 3950−3955.
(11) Vijayakumar, S.; Nagamuthu, S.; Muralidharan, G. *ACS Appl. Mater. Interfaces* **2013**, *5* (6), 2188−2196.
(12) Xing, W.; Li, F.; Lu, G. Q. *J. Power Sources* **2004**, *134*, 324−330.
(13) Yu, C.; Zhang, L.; Shi, J.; Zhao, J.; Gao, J.; Yan, D. *Adv. Funct. Mater.* **2008**, *18*, 1544−1554.
(14) Wang, Y. G.; Xia, Y.-Y. *Electrochim. Acta* **2006**, *51*, 3223−3227.
(15) Zheng, Y. Z.; Zheng, M.-L. *Mater. Lett.* **2007**, *61*, 3967−3969.
(16) Liu, H. B.; Xiang, L.; Jin, Y. *Cryst. Growth Des.* **2006**, *6*, 283−286.
(17) Xu, L.; Ding, Y. S.; Chen, C. H.; Zhao, L.; Rimkus, C.; Joesten, R.; Suib, S. L. *Chem. Mater.* **2008**, *20*, 308−316.
(18) Li, J.; Zhao, W.; Huang, F.; Manivannan, A.; Wu, N. *Nanoscale* **2011**, *3*, 5103−5109.
(19) Sicard, L.; Llewellyn, P. L.; Patarin, J.; Kolenda, F. *Microporous Mesoporous Mater.* **2001**, *44*−*45*, 195−201.
(20) Kuang, D. A.; Lei, B. X.; Pan, Y. P.; Yu, X. Y.; Su, C. Y. *J. Phys. Chem. C* **2009**, *113*, 5508−5513.
(21) Liu, J.; Guo, Z.; Meng, F.; Jia, Y.; Luo, T.; Li, M.; Liu, J. *Cryst. Growth Des.* **2009**, *9*, 1716−1722.
(22) Meher, S. K.; Justin, P.; Rao, G. R. *Nanoscale* **2011**, *3*, 683−692.
(23) Yan, J.; Khoo, E.; Sumboja, A.; Lee, P. S. *ACS Nano* **2010**, *4*, 4247−4255.
(24) Saravanakumar, B.; Purushothaman, K. K.; Muralidharan, G. *ACS Appl. Mater. Interfaces* **2012**, *4*, 4484−4490.
(25) Wang, N.; Wu, C.; Li, J.; Dong, G.; Guan, L. *ACS Appl. Mater Interfaces* **2011**, *3*, 4185−4189.
(26) Zheng, Y. Z.; Ding, H. Y.; Zhang, M. L. *Mater. Res. Bull.* **2009**, *44*, 403−407.
(27) Meher, S. K.; Justin, P.; Rao, G. R. *Electrochim. Acta* **2010**, *55*, 8388−8396.
(28) Srinivasan, V.; Weidner, J. W. *J. Electrochem. Soc.* **2000**, *147*, 880−885.
(29) Liu, C.; Yu, Z.; Neff, D.; Zhamu, A.; Jang, B. Z. *Nano Lett.* **2010**, *10*, 4863−4868.
(30) Fan, L.; Tang, L.; Gong, H.; Yao, Z.; Guo, R. *J. Mater. Chem.* **2012**, *22*, 16376−16381.
(31) Xu, M. W.; Bao, S. J.; Li, L. *J. Solid State Electrochem.* **2007**, *11*, 372−377.
(32) Conway, B. E. *Electrochemical Supercapacitors: Scientific Fundamentals and Technological Applications*; Kluwer Academic/Plenum Press: New York, 1999; p 529.
(33) Zang, J. F.; Bao, S. J.; Li, C. M.; Bian, H. J.; Cui, X. Q.; Bao, Q. L.; Sun, C. Q.; Guo, J.; Lian, K. R. *J. Phys. Chem. C* **2008**, *112*, 14843−14847.